Respiratory Research

RESEARCH

Open Access

Whole genome comparisons reveal gut-to-lung translocation of *Escherichia coli* and *Burkholderia cenocepacia* in two cases of ventilator-associated pneumonia in ICU patients

Huihui Gao[1], Lei Xu[2], Yixin Liu[1], Xiaolong Wang[3], Siyuan Zhu[3], Huai Lin[4], Yuting Gao[3], Daqing Mao[1*], Xing Lu[2*] and Yi Luo[3,4*]

Abstract

Background Identifying the sources of pathogenic bacteria causing ventilator-associated pneumonia (VAP) in intensive care unit (ICU) patients is crucial for developing effective prevention and treatment strategies. However, the scarcity of reported cases with confirmed sources limits the ability to evaluate and manage VAP, which remains a major challenge for healthcare systems globally.

Methods Pathogens were isolated from endotracheal aspirate (ETA) samples of VAP patients using conventional culture techniques. Whole-genome comparisons, based on average nucleotide identity (ANI), were performed to identify genetically identical strains by comparing pulmonary isolate genomes with gut metagenome-derived bacterial genomes. Mouse models of pneumonia and colitis were used to validate the translocation of pathogenic bacteria from the gut to the lungs. Metagenomic analysis was performed to characterize the gut microbiome and resistome.

Results Pathogenic isolates were obtained from the ETA samples of seven VAP patients, with one isolate per sample. Among these, *Escherichia coli* (Ec1) and *Burkholderia cenocepacia* (Bc1) from two patients were genetically identical to strains in their respective gut microbiota, with ANI values above 99%, indicating gut-to-lung translocation. The Ec1 strain demonstrated increased resistance to cefazolin while remaining susceptible to gentamicin, amikacin, and kanamycin, compared to previously reported pneumonia-associated *E. coli* strains. The Bc1 strain showed elevated resistance to macrolides, chloramphenicols, and tetracyclines relative to pneumonia-associated *B. cenocepacia* strains.

*Correspondence:
Daqing Mao
maodq@nankai.edu.cn
Xing Lu
szxlx611818@126.com
Yi Luo
luoy@nankai.edu.cn

Full list of author information is available at the end of the article

Metagenomic analysis revealed a highly individualized gut microbiota composition among VAP patients. Notably, the translocated bacteria were not dominant within their gut microbiota. Additionally, these patients showed a marked increase in the total abundance of antibiotic resistance genes (ARGs) in their gut microbiota. The translocation ability of the Ec1 strain was validated in a mouse pneumonia model, where it caused more severe lung damage. Furthermore, elevated levels of *Escherichia-Shigella* were detected in the lung tissues of colitis mice, suggesting that gut-to-lung bacterial translocation may occur in a severely inflamed host, potentially leading to pneumonia.

Conclusions This study demonstrates the gut-to-lung translocation of *E. coli* and *B. cenocepacia*, highlighting their role in the development and progression of VAP in ICU patients. These findings provide valuable insights for implementing targeted prevention and treatment strategies for VAP in ICU settings.

Graphical abstract

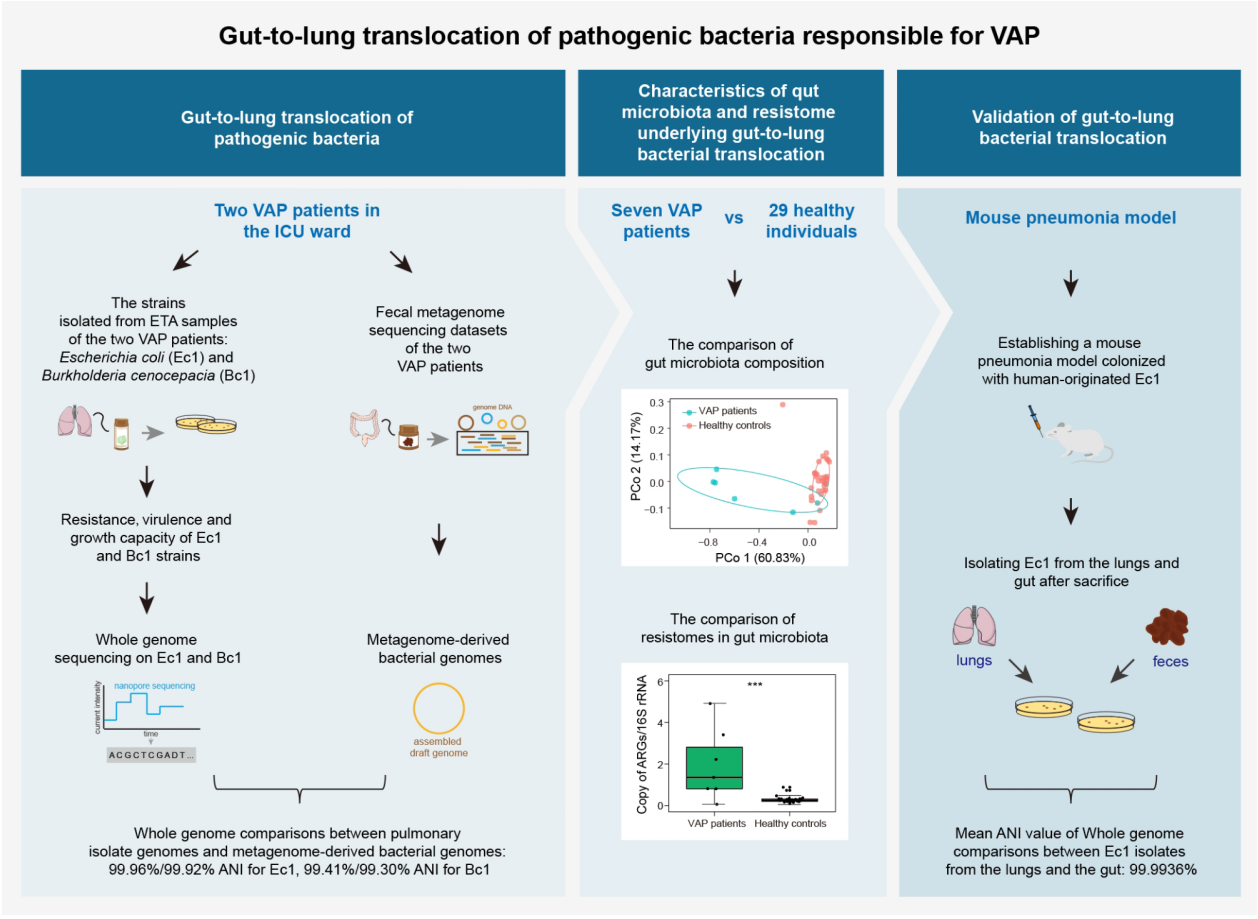

Keywords Gut-to-lung pathogen translocation, Ventilator-associated pneumonia, Comparative genomics, Gut microbiome, Metagenomics

Introduction

Ventilator-associated pneumonia (VAP) is a common nosocomial infection affecting lung tissues, typically occurring 48 h or more after the intubation of mechanical ventilation [1]. It is one of the most prevalent infections acquired in intensive care unit (ICU) and remains a significant contributor to morbidity and mortality [2]. According to the National Healthcare Safety Network, VAP accounts for 7–32% of healthcare-associated infections and 10% of pediatric device–related infections [3]. Pathogenic bacteria frequently implicated in VAP include both Gram-positive and Gram-negative species, such as *Staphylococcus aureus*, *Pseudomonas aeruginosa*, *Klebsiella*, and *Enterobacter* species [3, 4]. The precise sources of these pathogens are often unclear, posing challenges for the development of effective preventive strategies against VAP.

The etiology, epidemiology, pathophysiology, and treatment of VAP have been extensively studied for preventive and therapeutic purposes [5]. Previous studies often suggest that bacteria may reach the lungs through fecal contamination or by ascending migration from the intestines into the stomach, followed by aspiration into the lungs [6]. Despite significant efforts to enhance hygiene and reduce ICU-acquired infections, the incidence of VAP remains persistently high [7]. Beyond the reported causes, other overlooked factors may contribute to the development of ICU-acquired lung infections, warranting further investigation.

Recent studies have proposed the possibility of internal bacterial translocation from the gut across the intestinal barrier into the systemic or lymphatic circulation, ultimately reaching the lungs [8–10]. This hypothesis is supported by microbiome-level analyses comparing bacterial compositions in the lungs and gut of patients with acute respiratory distress syndrome, as well as in post-stroke mouse models [9, 10]. A notable study further substantiated this concept by identifying *P. aeruginosa* translocating from the gut to the lungs in an ICU patient through whole-genome comparisons of isolates obtained from traditional culture methods [11]. Despite these advances, the detection and characterization of translocated bacteria remain challenging due to the lack of effective screening labels for target organisms, making their isolation from complex gut microbial communities labor-intensive. Moreover, microbiome-level comparisons often fail to provide strain-level details, which are essential for understanding antibiotic resistance, physiological traits, and guiding therapeutic interventions. Consequently, gut-to-lung bacterial translocation via the gut-lung axis may be a contributing factor to VAP, the limited reports of this phenomenon in VAP patients could be attributed to methodological limitations.

Escherichia coli, predominantly from the B2 phylogenetic group, has been identified as a causative agent of ICU-associated pneumonia, characterized by a high virulence factor gene content and low antimicrobial resistance [12]. Recent data indicate that Enterobacteriaceae, particularly *E. coli*, are frequently implicated in ICU-associated pneumonia, with an incidence of approximately 6.64–10.52 isolates/1000 patient-days [13]. *Burkholderia cenocepacia*, a prominent member of the *Burkholderia cepacia* complex, is the second most common pathogen associated with lung infections in cystic fibrosis patients [14, 15]. Its virulence is underpinned by several key features, including the ability to acquire foreign DNA, regulate gene expression via quorum sensing, compete for iron during infection, and mediate antimicrobial resistance and inflammation through its membrane and surface polysaccharides [14]. Despite the clinical relevance of *E. coli* and *B. cenocepacia* in VAP, the specific sources of these pathogens within ICU environments remain unclear.

In this study, we employed whole-genome comparisons between pulmonary isolate genomes and gut metagenome-derived genomes to illustrate the gut-to-lung translocation. To further validate this translocation, we utilized a mouse pneumonia model colonized with human-originated *E. coli* and a DSS-induced colitis mouse model. These findings provide novel insights into possible pathways contributing to the development of VAP.

Materials and methods

Study population

This study included 36 eligible participants, consisting of seven VAP patients and 29 healthy controls. The VAP patients were recruited from the ICU at Tianjin Third Central Hospital, Tianjin, China, between December 2020 and June 2021. Inclusion criteria for VAP patients were individuals of any genders meeting the diagnostic criteria for VAP [16], while those with gastrointestinal disorders were excluded. All VAP patients underwent gut microbiota analysis, and their gut metagenome-derived draft genomes were compared with respective pulmonary isolate genomes using FastANI (https://github.com/ParBLiSS/FastANI). Only pathogens with ANI values ≥ 99% were selected for phenotypic experiments, those with ANI values < 99% were excluded. Gut microbiota datasets for healthy Chinese controls were obtained from the European Bioinformatics Institute (ERP005860) [17]. Control participants, age-matched to the VAP patients, were excluded if they had hypertension, diabetes, obesity, metabolic syndrome, inflammatory bowel disease, nonalcoholic fatty liver disease, celiac disease, cancer, or had received antibiotics/probiotics within 8 weeks of enrollment. Detailed participant information is provided in Table S1.

Isolation of pulmonary bacteria, nanopore sequencing and analysis

Endotracheal aspirate (ETA) samples were collected and stored at 4℃. MacConkey Agar Medium (Hope-Bio, HB8458, China) was used for pathogen isolation. Genomic DNA was extracted using the Bacterial Genome DNA Kit (CWbiotech, CW0552, China) following the manufacturer's instructions. DNA was then sent to Biomarker Technologies (Beijing, China) for sequencing on the Nanopore PromethION48 platform. Approximately 1 μg of DNA was employed for library construction with the Rapid Barcoding Sequencing Kit (Oxford Nanopore Technologies, SQK-RBK004, UK). Indexed libraries were loaded onto the flow cell and sequenced. Raw reads were base-called using guppy [18] and demultiplexed with qcat v. 1.1.0 (https://github.com/nanoporetech/qcat).

Filtered subreads were assembled with Canu v1.5 [19], followed by correction using Racon v3.4.3 [20]. Circularization and adjustment of starting points were performed with Circlator v1.5.5 [21], and final error correction was done using Pilon v1.22 [22]. The resulting high-accuracy genome was used for subsequent analysis.

Stool genomic DNA extraction

Fecal samples were collected by ICU physicians and immediately stored at -80 °C by assistants for further experiments. DNA was extracted from approximately 100 mg of fecal material using the QIAamp Fast DNA Stool Mini Kit (QIAGEN, 51604, Germany) following the manufacturer's instructions. DNA quality and integrity were assessed by 1.0% agarose gel electrophoresis, and concentrations were measured using a NanoPhotometer (IMPLEN, NanoPhotometer N60/N50, Germany).

Metagenomic sequencing and taxonomic profiling

Approximately 1 μg of DNA per fecal sample was used for library construction, followed by paired-end sequencing on an Illumina NovaSeq 6000 platform (PE150) at Novogene Bioinformatics Technology Co., Ltd. (Beijing, China). Raw sequencing data were trimmed, and human reads (hg38 human reference genome: http://hgdownload.cse.ucsc.edu/goldenPath/hg38/bigZips/hg38.fa.gz) were removed using Bowtie2 v2.4.4 (http://bowtie-bio.sourceforge.net/bowtie2/index.shtml). High-quality sequences were then assembled using Megahit (https://github.com/voutcn/megahit) [23]. Taxonomic profiling was performed using MetaPhlAn 3.0 [24] to assess the relative abundance of microbial species. A total of 258 bacterial species were identified in VAP patients, and 188 in healthy individuals (Table S2).

ARG annotation

For pathogens, ARG annotation was performed using CARD [25], a curated resource for AMR gene identification. Genomic sequences were analyzed using the Resistance Gene Identifier (RGI) tool provided by CARD, which utilizes the curated Antibiotic Resistance Ontology to predict ARGs based on sequence homology and protein family classification. Default parameters were applied to ensure accurate annotation, and only hits with strict or perfect matches to reference genes were retained. For gut metagenomes, the ARGs were determined using the ARGs-OAP v2.0 pipeline [26, 27]. As stated in the reference, the formula for calculating ARG abundance (copies of ARGs/16S rRNA gene) is as follows:

$$ARG\ abundance = \sum_{1}^{n} \frac{\frac{N_{ARG-like\ sequence} \times L_{reads}}{L_{ARG\ reference\ sequence}}}{\frac{N_{ARG-like\ sequence} \times L_{reads}}{L_{16S\ sequence}}}$$

Bacterial sampling and detection in the ward environment

Sterile cotton swabs, pre-moistened with pre-cooled sterile 1× PBS, were used to sample surgical instruments, countertops, floors, and doorknobs within the ward. Each swab was then placed into 200 μl of pre-cooled 1 × PBS in a 1.5 mL tube, ensuring full immersion. The resulting solution was spread onto LB agar plates and incubated at 37 °C for 24 h. After incubation, colony growth was assessed to determine the presence of pathogenic bacteria.

Assembling draft genomes based on reference genomes, and average nucleotide identity (ANI) estimate

The pulmonary pathogen genomes were established as reference genomes to extract corresponding draft genomes from gut microbiota. Indexing of reference genomes and alignment of fecal metagenomic data reads to these reference genomes were conducted with Bowtie2 v2.4.4. The aligned reads were assembled using SPAdes v3.13.1 (https://github.com/ablab/spades). Pairwise comparisons of complete pathogen genomes and gut metagenome-derived genomes were conducted using FastANI (https://github.com/ParBLiSS/FastANI). Genome mappings were visualized using an R script with the "genoPlotR" package, available in the repository (https://github.com/ParBLiSS/FastANI/tree/master/scripts).

De Novo assembly, Binning, and ANI estimate

Processed sequencing reads were de novo assembled using Megahit (https://github.com/voutcn/megahit), generating contigs with a minimum length of 200 bp. For binning, Bowtie2 (http://bowtie-bio.sourceforge.net/bowtie2/index.shtml), Samtools [28], and MetaBAT2 [29] were employed sequentially. Bowtie2 was utilized to align the reads to the assembled contigs, while Samtools converted and sorted the resulting alignment files. MetaBAT2 then partitioned the contigs into distinct bins based on coverage depth. To assess the quality and completeness of the assembled bins, checkM was applied [30]. The obtained bins were subsequently compared against reference pathogen genomes using BLASTn [31]. Finally, pairwise comparisons between complete pathogen genomes and draft genomes were performed using FastANI (https://github.com/ParBLiSS/FastANI).

Minimum inhibitory concentration (MIC) measurements

MIC measurements were conducted as previously described to assess the antibiotic resistance of translocated isolates [32]. *E. coli* Ec1 and *B. cenocepacia* Bc1 isolates were cultured overnight in 2 mL of LB broth (HopeBio, HB0128, China). The saturated cultures (20 μL) were then inoculated into 2 mL of fresh LB broth and sub-cultured to an OD of ~0.5 at 600 nm. The cultures were then transferred to 96-well plates containing

antibiotics (kanamycin (KAN), amikacin (AMK), gentamicin (GEN), ampicillin (AMP), imipenem (IPM), cefazolin (CZO), ceftazidime (CAZ), polymyxin B (poly B), polymyxin E (poly E), chloromycetin (CM), levofloxacin (LEVO), fosfomycin (FOS), erythrocin (ERY), azithromycin (AZM), moxifloxacin (MXF), tetracycline (TET)) in log2 serial dilutions, with an initial density of 5×10^5 CFUs/mL. After 24 h of incubation at 37 °C with shaking at 234 rpm, the OD600 was recorded.

Infection of galleria Mellonella larvae

G. mellonella killing assays were performed using K12 (standard *E. coli* K12 MG 1655), Ec1, Bc (standard *B. cenocepacia* ATCC BAA-245), and Bc1 strains. The K12 and Bc strains were purchased from Beijing Biosea Biotechnology co., LTD. Overnight cultures of each isolate were washed with 1 × PBS and adjusted to a concentration of 1×10^7 CFUs/mL. Ten larvae, each approximately 3 cm in length, were individually injected with 10 µL of the bacterial suspension for each strain. The larvae were then incubated in a 90 cm culture dish in the dark at 37 °C for 96 h. The quantity of dead larvae was recorded every 12 h. The assay was conducted with three biological replicates.

Growth curves

Bacterial growth curves were monitored using a microplate reader (BMG Labtech, POLARstar Omega, Germany). Each well of the honeycomb microplates was loaded with 198 µL of fresh LB broth and inoculated with 2 µL of the tested strains (K12, Ec1, Bc, and Bc1 strains, 5×10^8 CFUs/mL) [33]. The cultures were incubated at 37 °C with shaking at 200 rpm, and the bacterial concentration (OD600) was recorded every 0.5 h for a total of 24 h. Bacterial growth curve analysis and key metrics, including intrinsic growth rate, lag time, and maximum population density, were obtained using the *Grofit* package in R [34].

Animal experiments

All animal experiments followed ethical guidelines and were approved by the Institute of Radiation Medicine, Chinese Academy of Medical Sciences (Approval No. IRM/2-IACUC-2205-002). Eight-week-old male C57BL/6J mice (21 g), from Beijing Vital River Laboratory Animal Technology Co., Ltd, were acclimatized for one week and housed under standard specific-pathogen-free conditions at the Institute of Radiation Medicine. The housing conditions at 24–25 °C, 50–55% humidity, and a 12-hour light/dark cycle. For the pneumonia model, mice ($n = 5$ per group) were randomly assigned to four groups: Cont (Standard diet, *ad libitum* water for 30 days, followed by intratracheal instillation of 1 × PBS on day 31), Pa (Standard diet and water *ad libitum* for 30 days, followed by intratracheal instillation of *P. aeruginosa* (P8 W, 5×10^7 CFUs) on day 31), Ec (Standard diet and water *ad libitum* for 30 days, with Ec1 gavage every other day, followed by intratracheal instillation of 1 × PBS on day 31), and EcPa (Standard diet and water *ad libitum* for 30 days, with Ec1 gavage every other day, followed by *P. aeruginosa* instillation on day 31). To minimize contamination, oral cavity of each mouse was carefully cleaned with a fine 75% alcohol-soaked cotton swab prior to the *P. aeruginosa* challenge. Mice were sacrificed 12 h after the instillation, and tissue samples were collected and stored at -80 °C for further analysis. For the colitis model, mice ($n = 5$ per group) were assigned to Control (Standard diet and water ad *libitum* for 7 days) and 5% DSS (Standard diet and water *ad libitum* added with 5% DSS for 7 days) groups. After euthanasia, the Mesenteric Lymph Nodes (MLNs) and lung tissues were immediately homogenized for bacterial plating and cultivation. The remaining tissue samples were collected and stored at -80 °C for subsequent analysis.

Isolation of E. coli Ec1 from mouse tissues and whole-genome sequencing

After euthanasia, samples from the oral cavity, lungs and feces of mice were collected and stored in 1 × PBS solution. Ec1 (ampicillin-resistant *E. coli* strain) was selectively isolated using *E. coli* chromogenic medium (Hopebio, HB7001, China) with 100 mg/L ampicillin. Representative isolates underwent DNA extraction and purification using a Bacteria genomic DNA kit (CWbiotech, CW0552, China) following the manufacturer's instructions. A total of 1 µg of DNA was used for whole-genome sequencing at Biomarker Technologies. For whole-genome comparisons of isolates from mouse tissues, FastANI (https://github.com/ParBLiSS/FastANI) was applied.

Histological analysis

Colon and lung tissues were fixed in 4% paraformaldehyde, embedded in paraffin, and sectioned to 5 µm. The sections were stained with Hematoxylin and Eosin (H&E) (Solarbio, G1120, China). The colon histological damage score was based on evaluations of crypt architecture, inflammatory cell infiltration, muscle thickening, goblet cell depletion, and crypt abscesses [35]. Total lung damage score was the sum of scores for each criterion (lung injury areas, collapsed alveoli, hyperplasia and metaplasia of bronchial epithelial cells, mucus plugs defined as mucus material in bronchi and total inflammatory cells) [36].

Flow cytometry

For Th17 cell staining, lymphocytes isolated from the spleen were incubated with a cell stimulation cocktail

(plus protein transport inhibitors) (Thermo Fisher Scientific, 00-4975-93, USA) at 37 °C and 5% CO2 for 6 h. Surface staining was performed using FITC-anti-mouse CD3 (Thermo Fisher Scientific, 11-0032-80, USA), Percp-anti-mouse CD4 (BioLegend, 100537, USA), and Percp-anti-mouse CD45 (BioLegend, 103129, USA). For intracellular staining, cells were fixed and permeabilized with fixation/permeabilization solution (BD Biosciences, 554722, USA), followed by staining with APC-anti-mouse IL-17 A (BioLegend, 506915, USA). For Treg cell staining, lymphocytes were isolated from the spleen, MLNs and colon lamina propria. Surface markers FITC-anti-mouse CD3 (Thermo Fisher Scientific, 11-0032-80, USA), Percp-anti-mouse CD4 (BioLegend, 100537, USA), and APC-anti-mouse CD45 (BioLegend, 147707, USA) were used, along with the intranuclear staining marker PE-anti-mouse Foxp3 (Miltenyi Biotec, 130-111-678, Germany). Stained cells were then analyzed for proportions.

Statistical analyses

Statistical analyses were performed using R v4.1.0 (R Foundation for Statistical Computing, Austria, https://www.R-project.org/.) and GraphPad Prism v8.2.1.441 (GraphPad Software, USA). The Shannon and Simpson indices were calculated using the *vegan* R package [37]. Principal Coordinates Analysis (PCoA) based on the weighted UniFrac distance or Bray–Curtis dissimilarity was performed and visualized using the *vegan* [37], *ade4* [38], and *ggplot2* [39] R packages. The ANOSIM function in the *vegan* package [37], with 999 permutations, was employed to assess statistical significance. Heatmaps were generated using the *ggplot2* R package [39]. Procrustes analysis was performed using the *vegan* [37] and *ggplot2* [39] packages. Distinguishing biomarkers between groups were identified using the LEfSe analysis web tool (http://huttenhower.sph.harvard.edu/galaxy).

Results

Characteristics of pathogenic strains isolated from ETA samples

Two strains, *E. coli* (Ec1) and *B. cenocepacia* (Bc1), were isolated from endotracheal aspirate (ETA) samples from two out of seven VAP patients in ICU. Subsequent findings identified these strains as translocation bacteria. Antibiotic resistance testing revealed that Ec1 exhibited the highest resistance to ampicillin, imipenem, cefazolin, and azithromycin (Fig. 1A). Whole-genome sequencing of Ec1 identified 13 antibiotic resistance genes (ARGs), including genes for efflux pumps, β-lactamases, and membrane-repair mechanisms, contributing to resistance to multiple antibiotic classes (Fig. 1B). Additionally, Ec1 contained 62 potential virulence genes related to adhesion, invasion, and host survival, such as genes for flagella, pilus, capsule, and siderophores (Fig. 1C). Infection of *G. mellonella* larvae with Ec1 resulted in a survival rate of 41.7%, significantly lower than the 63.6% survival rate of *E. coli* K12 (Fig. 1D). Ec1 also showed faster growth and higher maximum population density than K12, with no significant difference in lag time and biofilm formation (Fig. 1E-I). Ec1 harbored four plasmids (Fig. S1).

For Bc1, the highest resistance was observed to ampicillin, imipenem, cefazolin, and ceftazidime (Fig. 1A). Whole-genome analysis identified efflux pump genes and β-lactamase genes (Fig. 1B), as well as virulence factors such as genes for flagella, capsule, and quorum-sensing systems (Fig. 1C). *G. mellonella* larvae infected with Bc1 exhibited a survival rate of 18.2%, which was lower than the 25.4% survival rate for standard *B. cenocepacia* (Bc) (Fig. 1D). Growth analysis showed Bc1 had a shorter lag phase and higher maximum biomass compared to Bc, although the growth rate was not significantly different (Fig. 1E-H). Biofilm formation between Bc1 and Bc was also not significantly different (Fig. 1I). Bc1 contained two plasmids (Fig. S2).

Pathogens isolated from the other five patients included *P. aeruginosa* (Pa1), *Enterococcus faecium* (Ef1), *Klebsiella pneumoniae* (Kp1), and *B. cenocepacia* (Bc2, Bc3), with their characteristics shown in Fig. S3. Comparisons of their genomes with draft genomes from their respective gut metagenomes revealed ANI values below 99%, suggesting that these isolates were likely not to be translocated bacteria.

Characteristics of gut microbiota in VAP patients

We analyzed the gut microbiota composition in seven VAP patients at multiple taxonomic levels. Healthy controls displayed a higher proportion of Bacteroidetes (48.32-83.01%) and a lower proportion of Firmicutes (15.00-48.38%). In contrast, VAP patients exhibited distinct microbiota patterns. Patients 1, 2, and 3 had microbiota compositions dominated by >98% Firmicutes, while patients 4 and 7 exhibited higher proportions of Bacteroidetes (Fig. 2A). At the family level, Bacteroideaceae predominated in healthy controls (40.66-79.52%), whereas VAP patients showed greater variability. Enterococcaceae were most abundant in patients 1, 2, and 6, while patient 3's microbiota was almost entirely composed of Leuconostocaceae (Fig. 2B). At the genus level, *Enterococcus* was abundant in several patients, with *Weissella* dominating in patient 3 (Fig. 2C). Species-level analysis revealed greater inter-patient diversity, but *E. faecium* was predominant in patients 1, 2, and 6 (Fig. S4).

We also performed statistical comparisons between the gut microbiota of VAP patients and healthy controls. α-diversity analysis revealed significant differences, with VAP patients showing a reduced Shannon index (Fig. 3A). PCoA and ANOSIM confirmed distinct

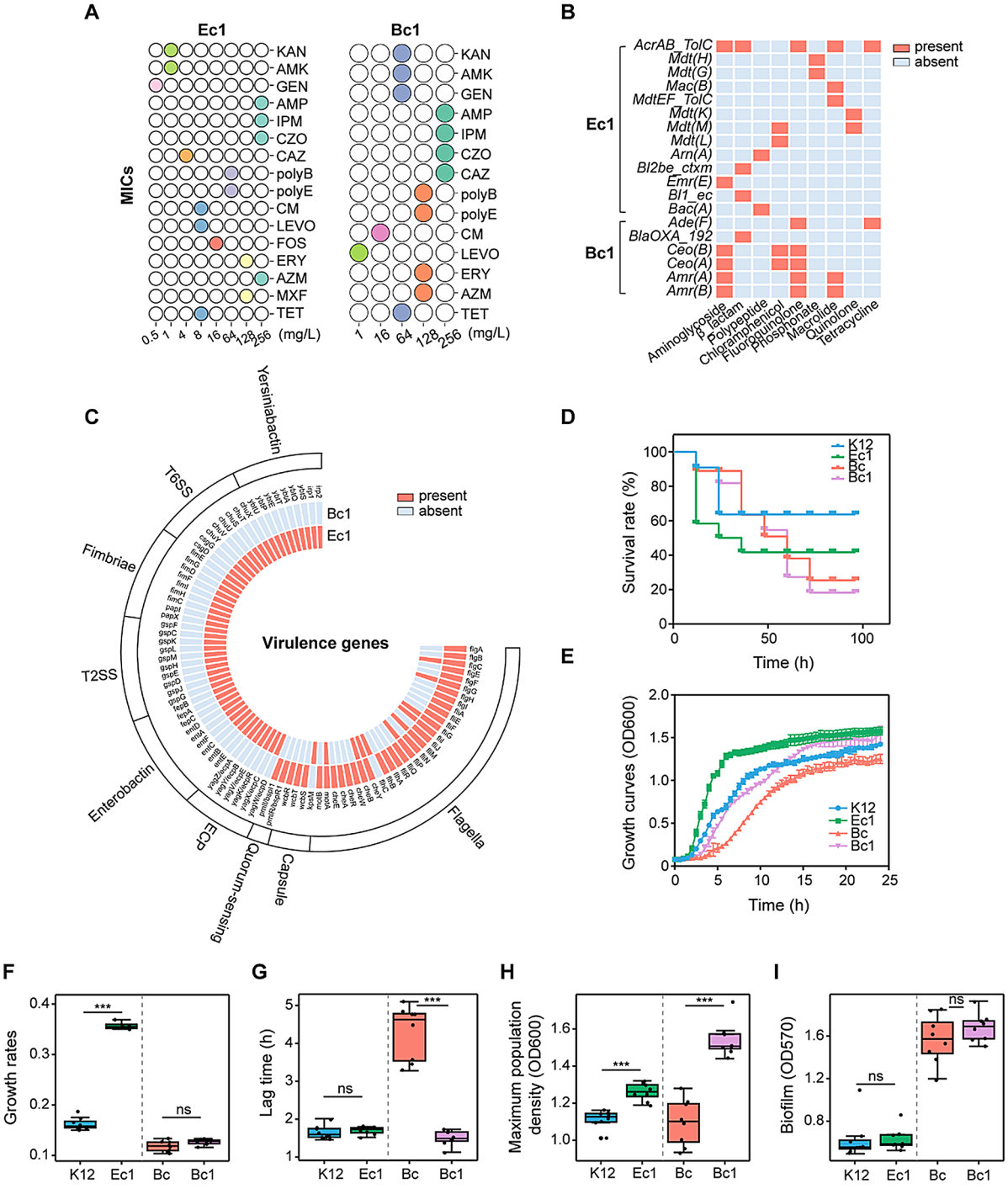

Fig. 1 (See legend on next page.)

(See figure on previous page.)

Fig. 1 Characteristics of Ec1 and Bc1 strains isolated from ETA samples of two VAP patients. (**A**) MIC values for the Ec1 and Bc1 strains against various antibiotics are represented by solid circles. Aminoglycosides: kanamycin (KAN), amikacin (AMK), gentamicin (GEN); β_lactams: ampicillin (AMP), imipenem (IPM), cefazolin (CZO), ceftazidime (CAZ); Polypeptides: polymyxin B (poly B), polymyxin E (poly E); Chloramphenicols: chloromycetin (CM); Fluoroquinolones: levofloxacin (LEVO); Phosphonate: fosfomycin (FOS); Macrolides: erythrocin (ERY), azithromycin (AZM); quinolone: moxifloxacin (MXF); Tetracyclines: tetracycline (TET). (**B**) ARG profiles of Ec1 and Bc1 strains and their resistance to the antibiotic classes (orange present, azure absent). (**C**) Binary heatmap showing the presence (orange) or absence (azure) of virulence genes in Ec1 and Bc1 strains. (**D**) Survival curves of *G. mellonella* larvae infected with K12, Ec1, Bc and Bc1 strains for 96 h. The blue, green, orange, and purple curves represent the survival rates of larvae infected with K12, Ec1, Bc and Bc1, respectively. (**E**) Growth curves of K12 (blue), Ec1 (green), Bc (orange), and Bc1 (purple) strains, with eight replicates per strain ($n = 8$). (**F**) Growth rate differences among K12, Ec1, Bc and Bc1 strains, calculated using the R package (*Grofit*) from the growth curve data. (**G**) Box plot illustrating the lag time (h) during growth for K12, Ec1, Bc, and Bc1 strains. (**H**) Box plot illustrating the maximum optical density (OD600) reached during growth for K12, Ec1, Bc, and Bc1 strains. (**I**) Box plot displaying biofilm formation (OD570) of K12, Ec1, Bc and Bc1 strains, with eight replicates per strain ($n = 8$). Statistics by the unpaired two-tailed Student's t test. Values shown are the mean ± SD. *** $p < 0.001$. *ns*: no significance. K12: standard *E. coli* K12 MG1655, Ec1: translocated *E. coli*, Bc: standard *B. cenocepacia*, Bc1: translocated *B. cenocepacia*

β-diversity between VAP patients and controls (Fig. 3B and C, $R = 0.778$, $p < 0.001$). At the phylum level, VAP patients exhibited an increased in Firmicutes and a decreased in Bacteroidetes, leading to a 4.43-fold increase in the Firmicutes/Bacteroidetes ratio (Fig. 3D). At the family level, Enterococcaceae were enriched, while Bacteroidaceae declined (Fig. 3E). *Enterococcus* abundance was higher at the genus level, with reductions in *Bacteroides* and short-chain fatty acid-producing genera such as *Roseburia* and *Faecalibacterium* (Fig. 3F). LEfSe analysis further highlighted these microbiota alterations (Fig. 3G). Additionally, pathogen species and abundance were elevated in VAP patients, with notable increases in *E. faecium* and other four pathogens (Fig. 3H-J). Overall, VAP patients showed gut microbiota alterations, characterized by a depletion of beneficial bacteria and an overgrowth of pathogenic species.

Gut resistome in VAP patients

Therapeutic antibiotics use affects the antibiotic resistance of intestinal flora. Analysis of fecal metagenome datasets identified 294 ARG subtypes in VAP patients (Table S3). While the number of ARG subtypes didn't differ significantly between VAP patients (82–195 subtypes) and healthy controls (75–162 subtypes) (Fig. 4A), the relative abundance of ARGs, measured as copies per 16 S rRNA gene, was markedly higher in VAP patients (0.06–4.91) compared to healthy controls (0.10–0.88) (Fig. 4B). Shannon diversity indices indicated comparable α-diversity between the two groups (VAP: 2.17–2.98, controls: 1.77–3.80, Fig. 4C). However, PCoA based on Bray-Curtis dissimilarity revealed significant differences in resistome between the two groups (Fig. 4D).

In VAP patients, ARGs conferring resistance to bleomycin, rifamycin, fosfomycin, vancomycin, bacitracin, aminoglycosides, multidrug, β-lactam, macrolide-lincosamide-streptogramin (MLS), tetracycline, and chloramphenicol classes were significantly enriched (Fig. 4E, Fig. S5, and Table S4). Notably, *Tet*(*Q*/*W*/*O*/*X2*) and *Erm*(*B*) genes were present in higher abundance compared to controls (Fig. 4F).

Taxonomic annotation of ARG-carrying contigs revealed Firmicutes, Proteobacteria, Actinobacteria, and Bacteroidetes as the primary reservoirs among 345 ARG-carrying contigs. Firmicutes accounted for 57% of these bacteria, predominantly carrying resistance genes for multidrug, MLS, aminoglycoside, tetracycline, and vancomycin classes (Fig. S6). Procrustes analysis revealed a significant correlation between ARGs and gut pathogens (Table S5) in VAP patients ($M^2 = 0.774$, $p < 0.001$, 9999 permutations) (Fig. 5A). Spearman correlation analysis further revealed positive associations between ARGs and 25 pathogens, including members of the *Enterococcus* genus. *E. faecium* exhibited strong correlations with nine ARG types, including aminoglycoside, bacitracin, β-lactam, chloramphenicol, fosfomycin, MLS, multidrug, tetracycline, and vancomycin (Fig. 5B). These findings underscore the role of pathogenic bacteria, particularly *Enterococcus* species, as major reservoirs of ARGs, which may compromise the effectiveness of antibiotics in VAP patients.

Gut-to-lung translocation of pathogenic bacteria in VAP patients

The ICU ward operates under positive pressure and undergoes twice-daily disinfection, with no pathogenic bacteria detected in the environment (e.g., surgical instruments, countertops, floors, and doorknobs). Stringent precautions were implemented to minimize procedural contamination. Based on these controls, we hypothesized that bacterial translocation via the gut-lung axis contributed to VAP. To test this hypothesis, we attempted to isolated identical strains from patient feces using antibiotic resistance markers but were unsuccessful. Instead, we utilized gut metagenome sequencing datasets to assemble bacterial genomes and performed whole-genome ANI analysis to compare bacterial genomes between the lungs and gut. ANI values greater than 99% between two genomes indicate a common ancestor, as previously reported [40]. Our comparisons revealed genetically identical strains between the lungs and the gut. Using reference-based methods to obtain draft genomes, the ANI values were 99.96% for *E. coli*

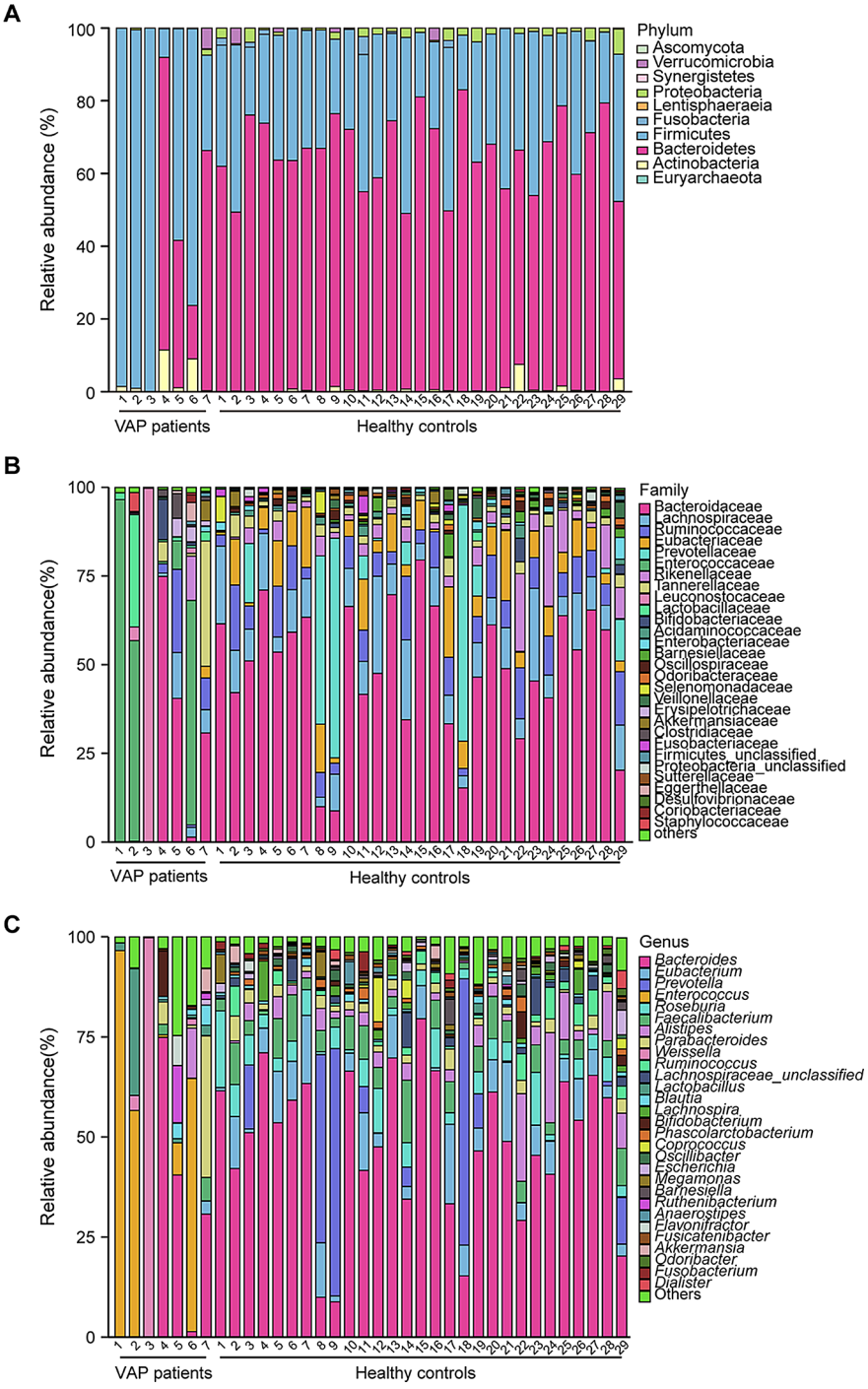

Fig. 2 High interindividual diversity in fecal microbiota composition at the phylum (**A**), family (**B**) and genus (**C**) level in VAP patients. Each bar represents the microbiota composition of one individual. The data are presented as the percentage of bacterial relative abundance in each sample

and 99.41% for *B. cenocepacia* (Fig. 6A and B). When draft genomes were obtained through de novo assembly and binning, the ANI values were 99.92% for *E. coli* and 99.30% for *B. cenocepacia* (Fig. 6C and D). These findings suggest that gut bacteria migrate to the lungs and contribute to the onset of VAP in these patients.

Gut-to-lung translocation of pathogenic bacteria in pneumonia and colitis mouse models

To confirm gut-to-lung translocation and explore the underlying mechanisms in mice, we colonized the gut with Ec1 and then induced lung infection through intratracheal infusion of *P. aeruginosa* (Fig. 7A). Ec1, identifiable using *E. coli* chromogenic medium with 100 mg/L

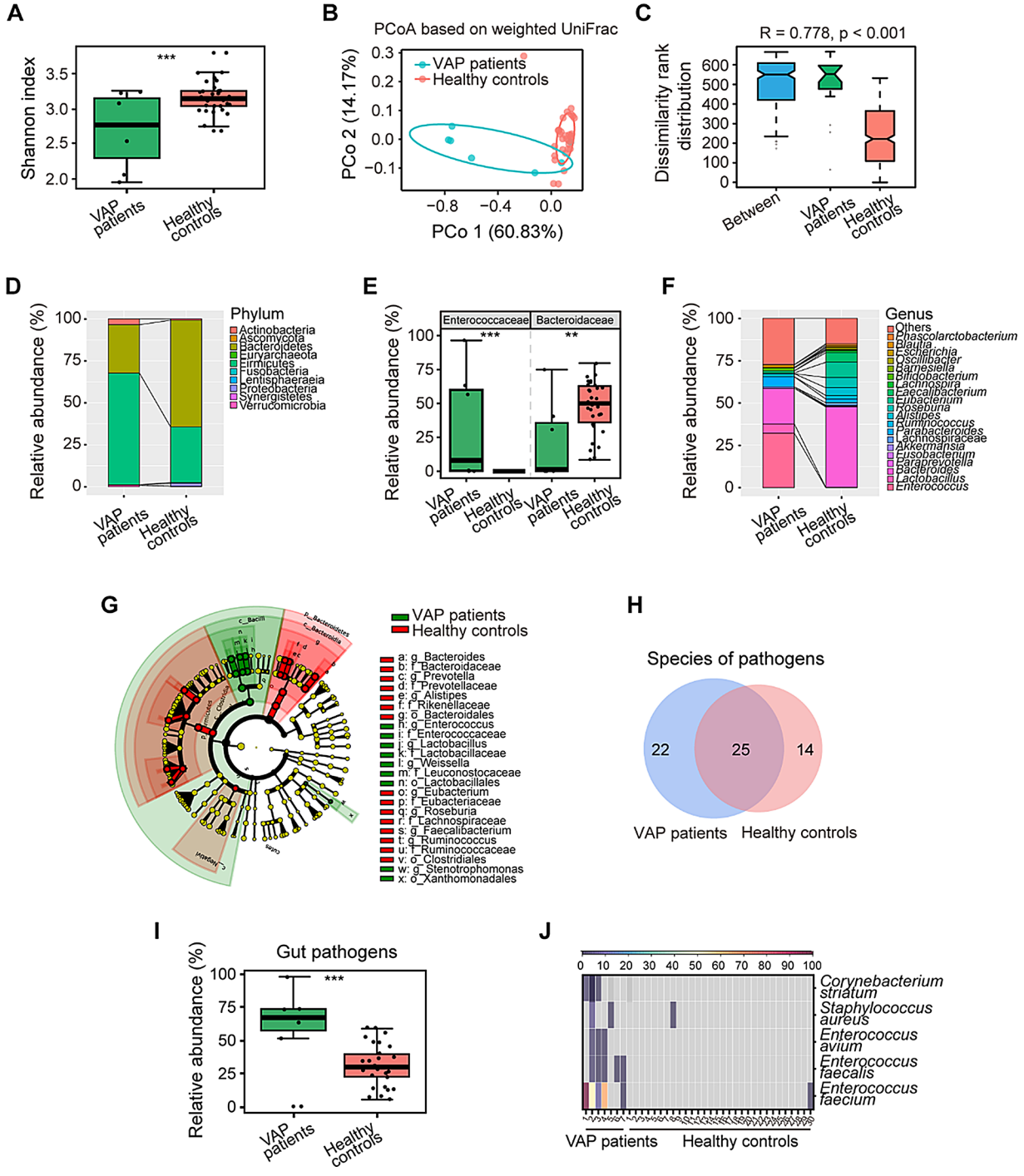

Fig. 3 Gut microbiota composition in VAP patients compared to healthy controls. (**A**) Box plot showing differences in gut microbial α-diversity, measured by the Shannon index, between VAP patients and healthy controls. (**B**) PCoA plot illustrating the distribution of gut microbiota composition based on β-diversity using weighted UniFrac distances. (**C**) ANOSIM analysis indicating distinct separation in gut microbiota composition between VAP patients and healthy controls ($R = 0.778$, $p < 0.001$). (**D**) Stacked bar plot of the average relative abundance of bacterial phyla in fecal samples from VAP patients and healthy controls. (**E**) Box plot comparing the relative abundance (%) of Enterococcaceae and Bacteroidaceae between the two groups. (**F**) Stacked bar plot depicting the relative abundance (%) of the top 20 bacterial genera in VAP patients and healthy controls. (**G**) Cladogram from LEfSe analysis highlighting microbial taxa enriched in VAP patients (green nodes) and healthy controls (red nodes). Yellow nodes represent taxa with no significant differences between groups. (**H**) Venn diagram of pathogenic species in fecal samples, showing 47 species in VAP patients, 39 species in healthy controls, and 25 species shared between the groups. (**I**) Box plot comparing the relative abundance (%) of pathogenic bacteria in the gut between VAP patients and healthy controls. (**J**) Heatmap of significantly different pathogenic bacteria between VAP patients and healthy controls across individual samples. Statistical analysis was performed using an unpaired two-tailed Student's t test. Data are presented as mean ± SD. ** $p < 0.01$, *** $p < 0.001$

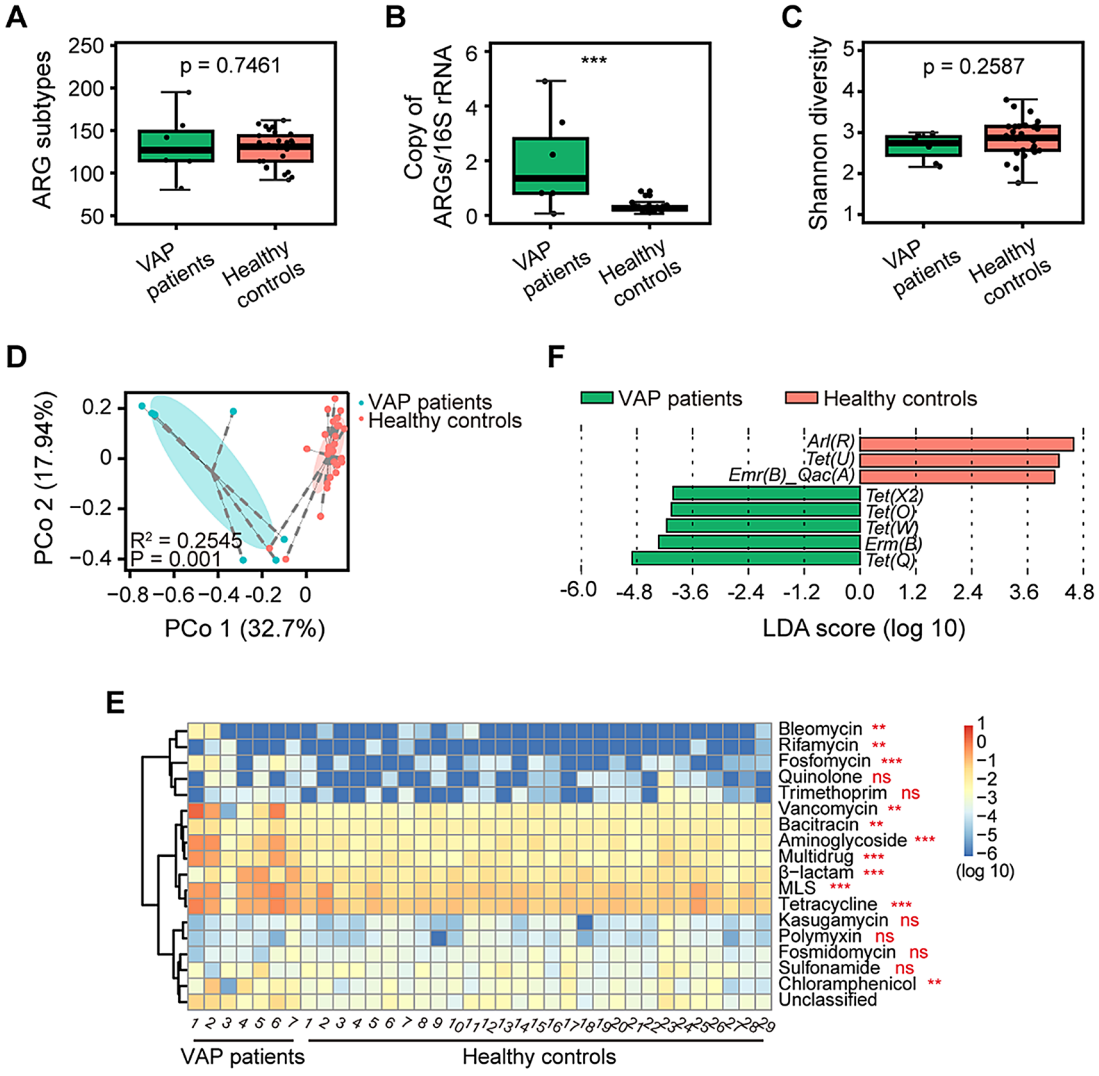

Fig. 4 Variations in the gut resistome of VAP patients compared to healthy controls. (**A**) Comparison of ARG subtype species between VAP patients and healthy controls. No significant difference was observed between the two groups ($p = 0.6308$). (**B**) The total relative abundance of ARGs was significantly higher in the gut of VAP patients compared to healthy controls, as indicated by the copies of ARGs/16S rRNA gene. (**C**) Box plot illustrating the Shannon index for ARGs in the gut microbiota of VAP patients and healthy controls. Although no significant difference was detected ($p = 0.1956$), a trend toward lower diversity was observed in patients. (**D**) PCoA plot based on Bray-Curtis dissimilarity, displaying the distribution of ARG profiles in the gut microbiota of VAP patients and healthy controls. (**E**) Heatmap presenting the profiles of different ARG types, assessed by $\log^{10}$ ARGs/16S rRNA, highlighting distinct antibiotic resistance patterns between VAP patients and healthy controls. Statistical differences are marked in red next to each ARG type. (**F**) Histogram showing linear discriminant analysis (LDA) scores from LEfSe analysis of ARGs in the gut microbiome. The LDA score is greater than 4.0. Statistics by the unpaired two-tailed Student's t test. Values shown are the mean ± SD. ** $p < 0.01$. *** $p < 0.001$. ns: no significance

ampicillin, was isolated from the lungs and gut of EcPa mice but was absent in oral samples (Fig. 7B and C). These findings indicate the translocation of Ec1 from the gut to the lungs. This conclusion is further supported by comparative genomic analysis. In the EcPa group, genomes of fecal isolates ($n = 3$, one isolate per mouse) showed over 99.9% ANI values with the original Ec1 strain (Fig. 7D and S7). Similarly, lung isolates ($n = 6$, two isolates per mouse) also exhibited over 99.9% ANI values with the original Ec1 (Fig. 7E and S8). Moreover, ANI values between lung and fecal isolates exceeded 99.9% (Fig. 7F-K), providing compelling evidence for Ec1 translocation in mice with *P. aeruginosa*-induced pneumonia.

To assess the impact of Ec1 colonization and translocation on lung injury, we performed H&E staining of lung tissues, which revealed more pronounced inflammatory infiltrates in the alveolar areas of EcPa mice compared to controls (Fig. 7L). Disease severity, evaluated using the disease activity index (Fig. 7M) and histological score (Fig. 7N), was higher in the EcPa group, suggesting that Ec1 colonization and translocation exacerbates lung inflammation. In the Ec group, slight lung damage was

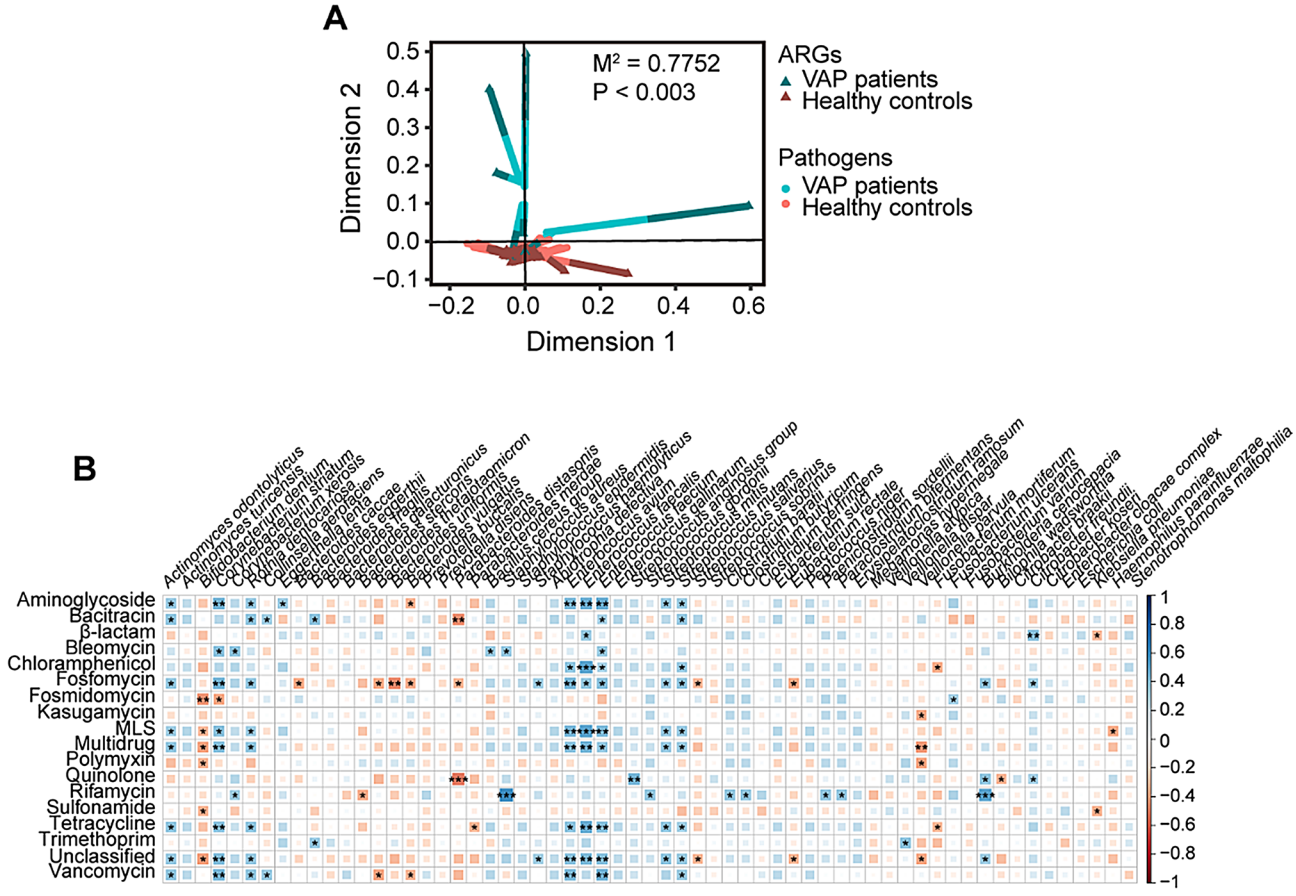

Fig. 5 Correlation between gut pathogen abundance and ARG profiles. (**A**) Multivariate Procrustes analysis comparing the gut pathogen composition with ARG type profiles of the participants. Shorter lines between an ARG eigenvalue (triangle) and its corresponding pathogen eigenvalue (round) indicate minor discordance between datasets for that sample. Significant correlations ($p < 0.001$, 9999 permutations) were detected. (**B**) Heatmap illustrating Spearman correlation analysis, representing statistically significant correlations between gut pathogens and ARG types. Blue squares indicate significant positive correlations ($r > 0.5$, $p < 0.05$), while orange squares indicate significant negative correlations ($r < -0.5$, $p < 0.05$). * $p < 0.05$. ** $p < 0.01$. *** $p < 0.001$

observed, possibly due to the translocation of pathogen-associated molecular patterns or immune cells, resulting in minor inflammation. Notably, antibiotic-resistant *E. coli* was cultured from the mesenteric lymph nodes (MLNs), while blood cultures remained negative, suggesting that gut bacteria may translocate via the lymphatic system (Fig. 7O). In the Pa group, we observed a reduction in Treg cell populations in the spleen, MLNs, and colon lamina propria, alongside an increase in Th17 cell populations in the spleen compared to control (Fig. 8A-D), reflecting an imbalanced immune response induced by pneumonia. These immune disturbances were even more pronounced in the EcPa group (Fig. 8A-D), suggesting that Ec1 colonization and translocation further exacerbated immune dysregulation. Histological analysis of the colon revealed shorter crypts and more severe damage in the EcPa group (Fig. 8E-H), indicating compromised gut barrier integrity and potential bacterial translocation. Mild colon injury was also observed in the Pa group, likely due to systemic dissemination of *P. aeruginosa*.

To further investigate primary lung infection resulting from gut-to-lung translocation, we utilized a 5% DSS-induced colitis model [41]. DSS treatment led to crypt disruption and thickening of the muscularis mucosa and submucosa, confirming the successful establishment of colitis model (Fig. 9A). In DSS-treated mice, bacterial cultures from the MLNs were positive, whereas no cultures were detected in control mice (Fig. 9B). Blood cultures from both groups remained negative, indicating that the lymphatic system may also act as a pathway for gut-to-lung translocation in colitis mice. 16 S rRNA sequencing of lung tissues revealed no significant changes in α-diversity, but the Shannon index was decreased, and the Simpson index was increased in DSS-treated mice, indicating lung microbial dysbiosis (Fig. 9C and D). β-diversity analysis based on Bray-Curtis distances showed significant differences in lung microbiota composition between DSS-treated and control groups (Fig. 9E).

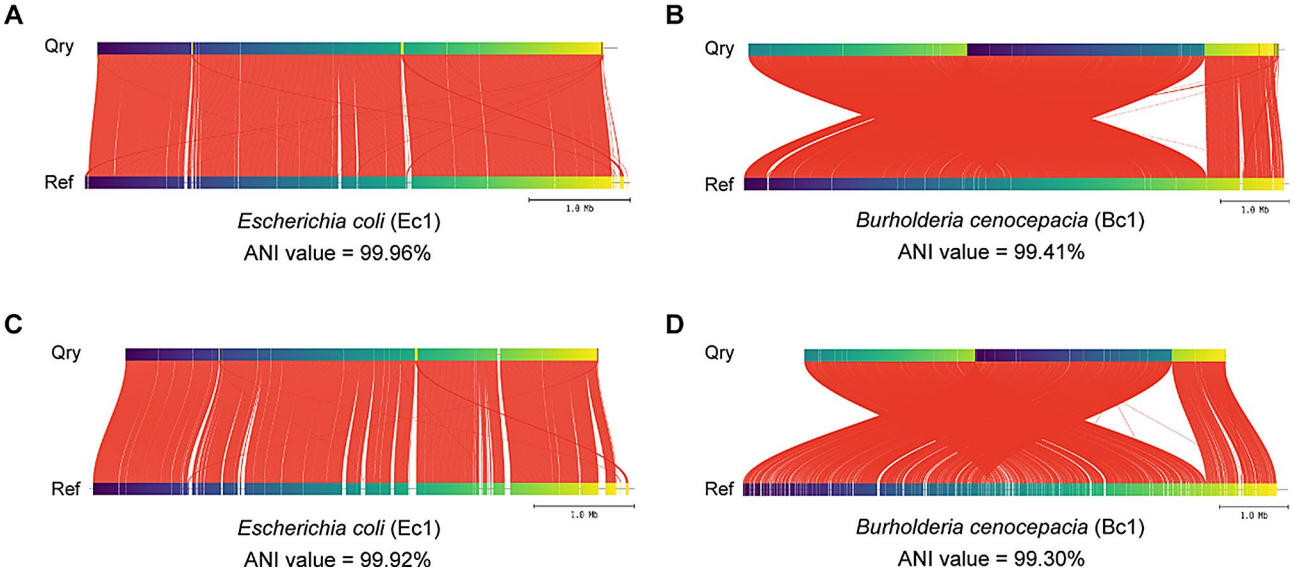

Fig. 6 ANI analysis of pulmonary isolate genomes and metagenome-derived genomes. The upper layer represents the assembled draft genomes, while the lower layer displays the reference genomes of the isolated strains. (**A**) The ANI value between the Ec1 genome and its corresponding assembled draft genome obtained utilizing reference genome-based methods is 99.96%. (**B**) The ANI value between the Bc1 genome and its corresponding assembled draft genome obtained utilizing reference genome-based methods is 99.41%. (**C**) The ANI value between the Ec1 genome and its corresponding assembled draft genome based on de novo assembly and binning is 99.92%. (**D**) The ANI value between the Bc1 genome and its corresponding assembled draft genome based on de novo assembly and binning is 99.30%. Ec1: translocated *E. coli*, Bc1: translocated *B. cenocepacia*

Notably, gut-associated bacteria, Enterobacteriaceae and *Escherichia-Shigella*, were significantly enriched in the lung tissues of DSS-treated mice (Fig. 9F and G). Positive bacterial cultures also detected in lung samples (Fig. 9H). Histological analysis of lung tissues demonstrated abscess formation, increased histological scores, and thickened alveolar septa (Fig. 9I). Additionally, total protein levels in bronchoalveolar lavage fluid (BALF) were significantly elevated in DSS-treated mice compared to controls (Fig. 9J). These findings suggest that Enterobacteriaceae and *Escherichia-Shigella* translocate to the lungs via lymphatic circulation in DSS-induced colitis mice, contributing to the initiation of lung inflammation.

Discussion

VAP is one of the most prevalent in ICU-acquired infections and remains a major contributor to hospital-acquired infection-related mortality, drawing considerable attention [2]. However, methodological limitations have hindered a comprehensive understanding of the origins of VAP-associated pathogens. Traditional bacterial isolation from complex gut microbial communities is labor-intensive and often impractical due to the lack of effective screening markers for translocated bacteria. Additionally, conventional microbiome analysis methods frequently fail to resolve strain-level critical phenotypic traits of pulmonary pathogens. To address these challenges, our study integrates culture-based isolation with whole-genome comparison approaches, linking pulmonary isolate genomes with gut metagenome-derived bacterial genomes. This approach enables the identification of gut-derived bacteria in the lungs without extensive culturing and allows for strain-level characterization of translocated pathogens. By providing detailed insights into their antibiotic resistance and virulence potential, our findings advance the understanding of bacterial translocation along the gut-lung axis and its role in VAP pathogenesis.

The ICU environment where patients were treated adhered to stringent infection control protocols. A positive-pressure ventilation system was designed to prevent the ingress of external airborne contaminants [42]. Regular and thorough disinfection procedures were implemented twice a day, encompassing patient areas, medical equipment, and surrounding environments. Environmental samples collected from surgical instruments, countertops, floors, and doorknobs tested negative for pathogens, effectively ruling out external contamination as a source of infection. Additionally, rigorous measures were taken to prevent procedural contamination. ICU medical staff strictly followed hand hygiene protocols and regularly change diapers and bed linens to prevent contamination by fecal microorganisms. Comprehensive oral care protocols, including the use of antiseptic mouthwash and plaque removal, effectively reduced the bacterial load in the oral cavity [43, 44]. Intubation was performed via a small neck incision, thereby bypassing the oral and pharyngeal regions where bacterial colonization is common [45]. This approach, combined with patient positioning practices such as head elevation [46], further mitigated

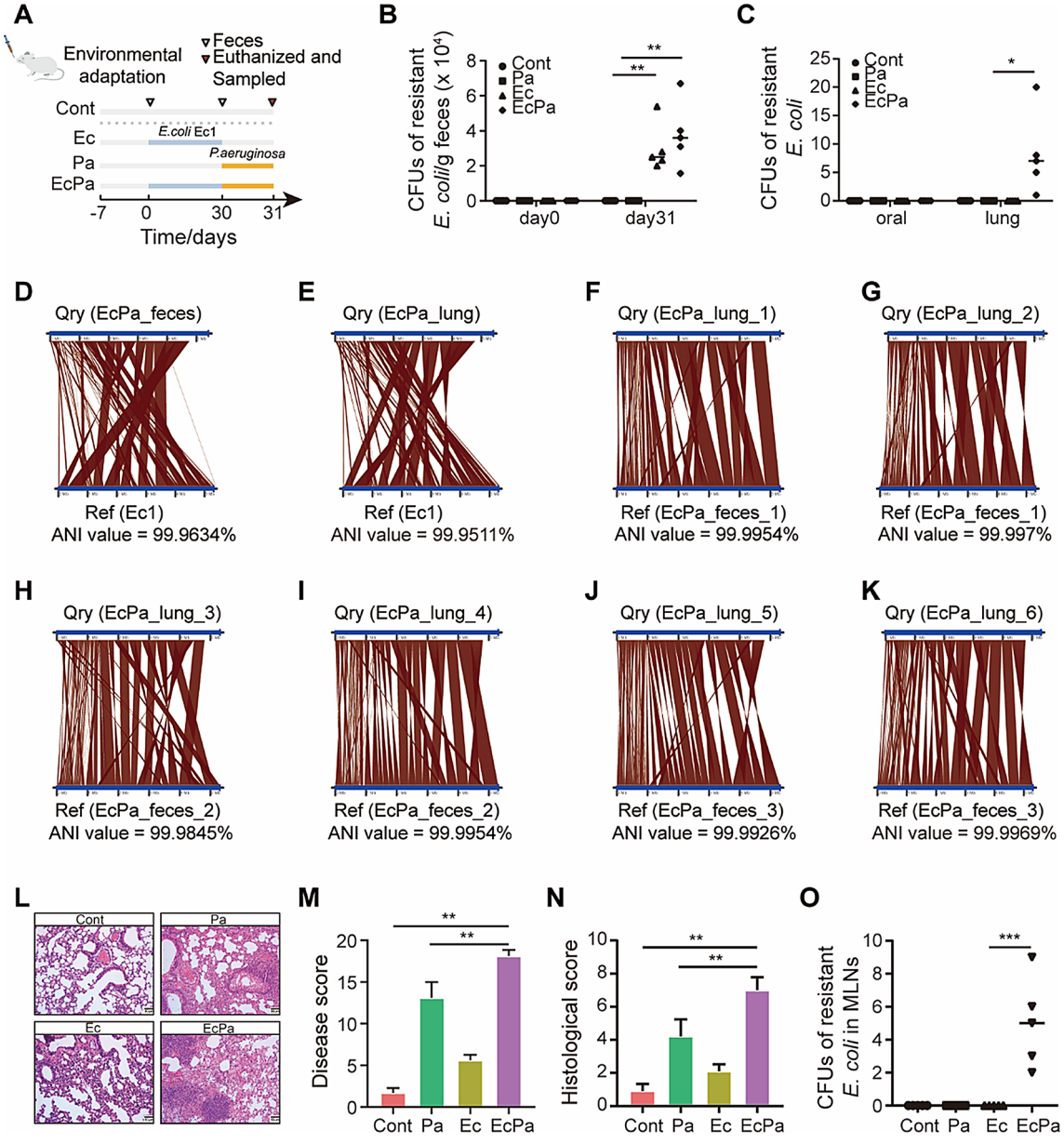

Fig. 7 Gut-to-lung translocation of antibiotic-resistant *E. coli* Ec1 in *P. aeruginosa*-induced pneumonia mice. (**A**) Experimental design and group assignments for mouse experiments. (**B**) Quantification of resistant *E. coli* Ec1 load in stool samples on days 0 and 31, cultured on *E. coli* chromogenic medium containing 100 mg/L ampicillin in the Cont, Ec, Pa, and EcPa groups ($n = 5$). (**C**) Quantification of resistant *E. coli* Ec1 load in the oral cavity and lung tissues after sacrifice, detected using *E. coli* chromogenic medium with 100 mg/L ampicillin across experimental groups ($n = 5$). (**D**) Representative image of ANI analysis comparing the genomes of resistant *E. coli* isolated from fecal samples of EcPa mice with the original Ec1 strain ($n = 3$). (**E**) Representative image of ANI analysis comparing the genomes of resistant *E. coli* isolated from lung tissues of EcPa mice with the original Ec1 strain ($n = 6$). (**F**-**K**) ANI analysis comparing resistant *E. coli* genomes isolated from lungs and fecal samples of EcPa mice, fecal isolates: $n = 3$, one isolate/mouse, lung isolates: $n = 6$, two isolates/mouse. (**L**) Representative H&E-stained lung sections from Cont, Ec, Pa, and EcPa groups. Scale bars = 50 μm ($n = 5$). (**M**) Disease activity index scores of lung injury across experimental groups ($n = 5$). (**N**) Histological score of lung injury based on H&E staining ($n = 5$). (**O**) Quantification of resistant *E. coli* Ec1 load in the MLNs after sacrifice, detected using *E. coli* chromogenic medium with 100 mg/L ampicillin across groups ($n = 5$). Statistics by one-way ANOVA with Tukey's post-hoc test. Values shown are the mean ± SD. * $p < 0.05$. ** $p < 0.01$. Ec1: translocated *E. coli*

the risk of aspiration or migration of oral or gastrointestinal bacteria into the lungs. Although gastroesophageal reflux was considered, the endotracheal tube cuff in the intubation device seals the trachea, preventing the aspiration of gastric contents, food particles, saliva, and other substances into the airway, thereby reducing the risk of aspiration pneumonia [47]. Consequently, pulmonary infections observed in this study could not be attributed to environment contamination or aspiration of oral

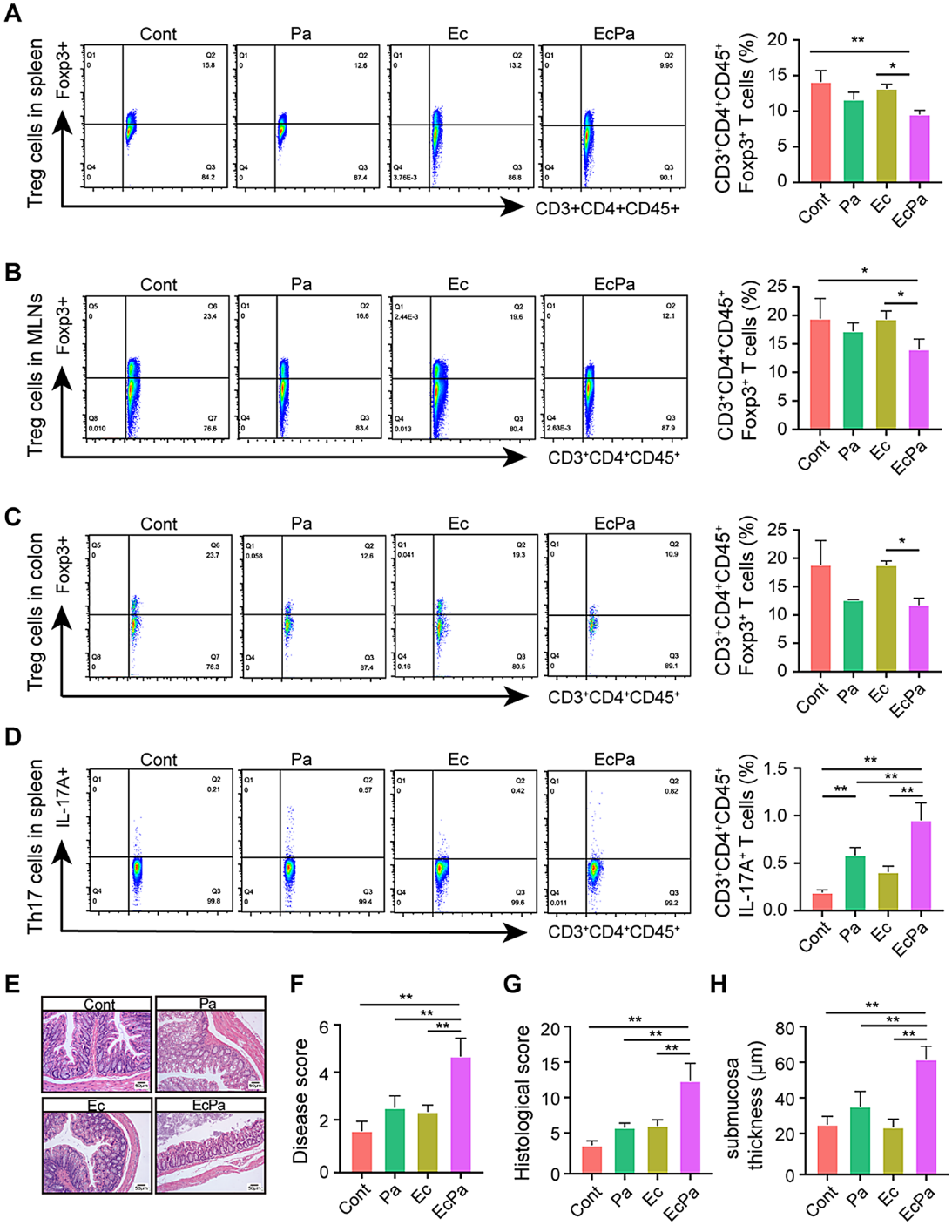

Fig. 8 Immunological changes and gut integrity in *P. aeruginosa*-induced lung infection mouse. (**A**-**C**) Representative flow cytometry plots and proportions of Tregs identified as FoxP3$^+$ within CD3$^+$CD4$^+$CD45$^+$ T cells in the spleen (**A**), MLNs (**B**), and colonic lamina propria (**C**) across experimental groups ($n = 3$). (**D**) Representative flow cytometry plots and proportions of Th17 cells identified as IL-17 A$^+$ within CD3$^+$CD4$^+$CD45$^+$ cells in the spleen across groups ($n = 3$). (**E**) Representative H&E-stained colon sections from Cont, Ec, Pa, and EcPa groups. Scale bars = 50 μm ($n = 5$). (**F**) Disease activity index scores indicating colon injury across groups ($n = 5$). (**G**) Histological score of colon injury from H&E-stained sections ($n = 5$). (**H**) Submucosa thickness (μm) of the colon in each group ($n = 5$). Statistics by one-way ANOVA with Tukey's post-hoc test. Values shown are the mean ± SD. * $p < 0.05$. ** $p < 0.01$

or gastrointestinal flora. Instead, our results suggest the direct migration of bacteria from the gut into the lungs.

From the ETA samples of seven patients, we isolated the dominant strain in each case. Among these, only *E. coli* Ec1 (isolated from patient 7) and *B. cenocepacia* Bc1 (isolated from patient 2) were identified as translocated bacteria through comparative genomic analysis, establishing them as key contributors to the development of

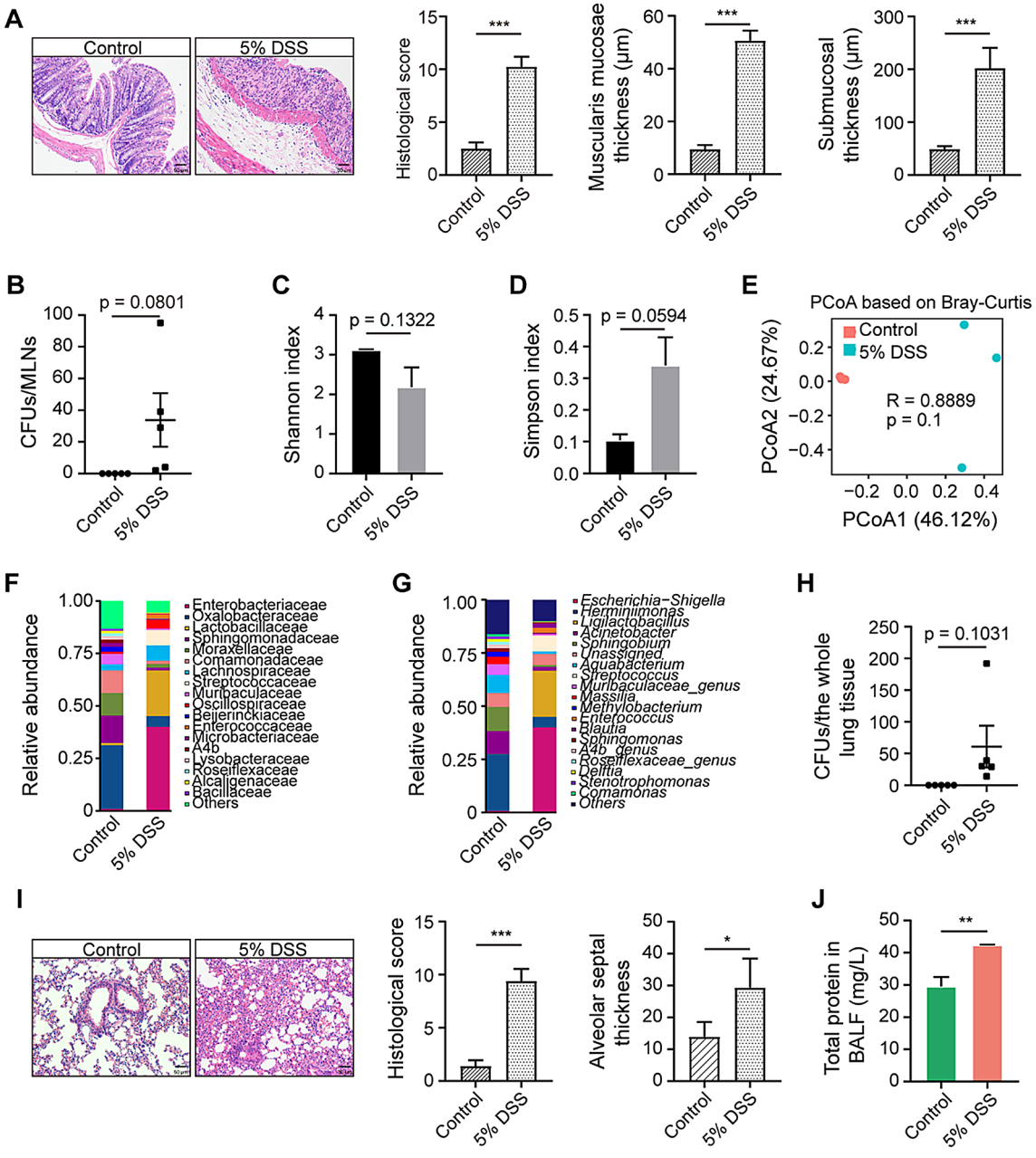

Fig. 9 Gut-to-lung translocation via the lymphatic system in DSS-induced colitis mice. (**A**) H&E staining of the distal colon to assess inflammation severity, with histological score, muscularis mucosae thickness, and submucosal thickness measurements. Scale bars = 50 μm ($n = 5$). (**B**) CFUs cultured from MLNs of Control and 5% DSS-treated mice ($n = 5$). (**C**, **D**) Box plots showing the α-diversity of lung microbiota in Control and 5% DSS groups, assessed using the Shannon (**C**) and Simpson indices (**D**) ($n = 3$). (E) PCoA plot displaying β-diversity of lung microbiota based on Bray-Curtis distances ($n = 3$). (**F**, **G**) Stacked bar plots presenting average relative abundance of bacteria taxa at the family (**F**) and genus (**G**) levels in lung microbiota from Control and 5% DSS-treated mice ($n = 3$). (**H**) CFUs cultured from whole lung samples of Control and 5% DSS-treated mice ($n = 5$). (**I**) H&E staining of lung sections to assess inflammation severity, with histological score and alveolar septum thickness measurements. Scale bars = 50 μm ($n = 5$). (**J**) Airway inflammation assessed by total protein concentration in bronchoalveolar lavage fluid ($n = 5$). Statistics by one-way ANOVA with Tukey's post-hoc test. Values shown are the mean ± SEM. * $p < 0.05$. ** $p < 0.01$. *** $p < 0.001$

VAP. Comparative genomics analysis of the remaining five isolate genomes with draft genomes yielded ANI values below 99%, likely due to insufficient coverage of the gut metagenomes [48]. Assembling fecal metagenomic-derived genomes based on reference genomes introduces potential confirmation bias, as only reads aligning exclusively to the ETA isolates are selected, omitting non-matching gene regions. And unlike de novo-assembled MAGs, using pulmonary genomes as reference genomes results in the alignment of a substantial number of

identical reads from fecal metagenomic to reference genome, whether it's the ancestor of this strain or not. Results from the mouse pneumonia model indicated that gut-to-lung bacterial translocation persisted following pneumonia onset, underscoring the need for physicians to consider ongoing translocation when devising therapeutic strategies for VAP. This study specifically verified the translocation of Ec1 from the gut to the lungs. Future investigations will focus on the translocation of Bc1 in mice, aiming to elucidate deeper mechanisms, including lung signaling interactions and shifts in microbial composition. In colitis models, we observed that gut-associated bacteria, Enterobacteriaceae and *Escherichia-Shigella*, appeared to translocate to the lungs via lymphatic circulation, potentially contributing to lung infections. However, the positive bacterial cultures in the lungs cannot be conclusively attributed to gut translocation. An alternative hypothesis is that these bacteria may naturally exist in the lungs at low, undetectable levels under normal conditions and proliferate in response to disease-induced changes. These findings highlight the intricate microbial interactions along the gut-lung axis and emphasize the importance of further research to clarify the mechanisms underlying these dynamics.

Although our study demonstrated that gut bacteria translocate to the lungs via lymphatic circulation in pneumonia and colitis mouse models, the precise mechanisms and routes of bacterial translocation in VAP patients remain unclear. Future investigations should focus on elucidating whether blood circulation, lymphatic drainage, or a combination of both serves as the primary route in the translocation process.

E. coli and *B. cenocepacia* have been recognized as pathogens associated with pneumonia [12, 49]. Previous studies have reported *E. coli* strains linked to pneumonia exhibiting resistance to multiple antibiotics, including ampicillin, levofloxacin, amoxicillin, ceftriaxone, imipenem, ciprofloxacin, cefotaxime, ceftazidime, gentamicin, amikacin, ofloxacin, piperacillin, and colistin [50–53]. In comparison, the Ec1 strain demonstrated increased resistance to cefazolin but remained susceptible to gentamicin, amikacin, and kanamycin. The *Burkholderia* genus is known for its intrinsic resistance to polymyxin, attributed to modified lipopolysaccharides [54]. Additionally, certain *Burkholderia* species exhibit resistance to fluoroquinolone and aminoglycoside due to alterations in DNA gyrase and the activity of efflux pumps [55]. Genomic analysis of *B. cenocepacia* has previously identified β-lactamase resistance genes (*PenB*, *AmpR*, *AmpC*, and *AmpD*) [56], and multidrug efflux pump genes (*AmrAB-OprA*, *BpeAB-OprB*, and *BpeEF-OprC*) [55]. Notably, the Bc1 strain in our study displayed a distinct ARG profile, encompassing macrolide (*AmrA*, *AmrB*), β-lactam (*BlaOXA-192*), tetracycline (*AdeF*), chloramphenicol (*CeoA*, *CeoB*), fluoroquinolone (*AdeF*, *AmrA*, *AmrB*, *CeoA*, *CeoB*), and aminoglycoside (*AmrA*, *AmrB*, *ceoA*, *ceoB*) resistance genes. These results highlight the substantial antibiotic resistance observed in *B. cenocepacia* and underscore the importance of considering these resistance profiles during the initial stages of empirical therapy.

Metagenomic analysis revealed that the gut microbiota composition of VAP patients was highly individualized, consistent with previous study on ICU patients [57]. However, an increased abundance of pathogenic bacteria was observed in these patients. This pathogen is of particular concern due to its association with high burdens of ARGs and its ability to produce toxins, which can complicate clinical management and worsen outcomes in VAP patients [58]. Interestingly, the translocated bacteria identified in our study were not the predominant members of the gut microbiota. This observation contrasts with previous research, which identified dominant gut species, *K. pneumoniae* and *E. faecium*, as translocated pathogens responsible for bloodstream infections [59]. This divergence underscores the complexity of gut-to-lung translocation and suggests that the mechanisms underlying this process in VAP may differ from those observed in bloodstream infections. Despite these complexities, the findings of this study provide valuable insights into the gut microbiome and resistome of VAP patients, offering potential guidance for antibiotic selection and therapeutic interventions.

Despite these results, further research involving larger longitudinal sampling and mechanistic studies is needed to confirm our findings, clarify the accuracy and mechanisms of gut-to-lung translocation, and further elucidate the role of the gut microbiota in the pathogenesis of VAP.

Our study highlights the critical role of gut-to-lung bacterial translocation in the development of lung infections among VAP patients. For the first time, we have identified the translocation of two specific species, *E. coli* and *B. cenocepacia*, from the gut to the lungs. These findings provide valuable insights that can inform the optimization of antibiotic therapy and the development of alternative therapeutic strategies targeting the gut microbiota for the treatment of VAP in ICU patients.

Conclusion

This study underscores the pivotal role of gut-to-lung bacterial translocation in the pathogenesis of VAP. Utilizing whole-genome comparison techniques, we successfully traced the migration of *E. coli* and *B. cenocepacia* from the gut to the lungs. These findings not only deepen our understanding of VAP etiology but also facilitate the development of more targeted and effective therapeutic interventions.

Abbreviations

VAP	Ventilator-associated pneumonia
ICU	Intensive care unit
ETA	Endotracheal aspirate
ANI	Average nucleotide identity
ARGs	Antibiotics resistance genes
MIC	Minimum inhibitory concentration
OD	Optical density
KAN	Kanamycin
AMK	Amikacin
GEN	Gentamicin
AMP	Ampicillin
IPM	Imipenem
CZO	Cefazolin
CAZ	Ceftazidime
poly B	Polymyxin B
poly E	Polymyxin E
CM	Chloromycetin
LEVO	Levofloxacin
FOS	Fosfomycin
ERY	Erythrocin
AZM	Azithromycin
MXF	Moxifloxacin
TET	Tetracycline
CFU	Colony-forming unit
H&E	Hematoxylin and Eosin
Th17 cell	T helper 17 cell
Treg cell	Regulatory T cell
IL-17A	Interleukin 17 A
MLNs	Mesenteric Lymph Nodes
ANOSIM	Analysis of Similarities
LEfSe	Linear Discriminant Analysis Effect Size
PCoA	Principal Coordinates Analysis
MLS	Macrolide-lincosamide-streptogramin

Supplementary Information

The online version contains supplementary material available at https://doi.org/10.1186/s12931-025-03204-x.

Supplementary Material

Acknowledgements

We thank the study participants for their dedication and time and the Tianjin Third Central Hospital for assistance with clinical samples.

Author contributions

Mao DQ and Luo Y designed the study; Xu L and Lu X collected the clinical samples; Gao HH, Wang XL, Zhu SY undertook the bioinformatic analysis; Gao HH, Liu YX, Lin H and Gao YT performed the animal experiments; Gao HH, Mao DQ and Xu L wrote the first draft of the manuscript; Mao DQ and Luo Y revised the manuscript. Gao HH and Mao DQ have accessed and verified the data, and Mao DQ were responsible for the decision to submit the manuscript. All authors read and approved the final manuscript.

Funding

This study was supported by the National Key R&D Program of China (2020YFC1806904), the Key Projects of the National Natural Science Foundation of China (41831287), the National Natural Science Foundation of China (42377426), the Tianjin Science and Technology Plan Project (18ZXDBSY00100), the Tianjin Municipal Natural Science Foundation (21JCYBJC01200), the Tianjin Graduate Research and Innovation Projects (2022BKY015) and the Research Project on Integrated Traditional Chinese and Western Medicine of Tianjin Municipal Health Commission (2023220).

Data availability

The sequencing data from this study have been deposited in the Genome Sequence Archive in BIG Data Center (https://bigd.big.ac.cn/), Beijing Institute of Genomics (BIG), China Academy of Sciences. The accession number of long-read and short-read sequencing data of pathogens are CRA012544 and CRA012543, respectively. The accession number of metagenomics sequencing data is CRA009715.

Declarations

Consent to participate

Not applicable. No consent to participate was required for using the clinical samples since they were collected during routine analysis in the hospital. Relevant documents about routine analysis have been provided as related file.

Consent to publish

Not applicable. All data were analyzed anonymously.

Competing interests

The authors declare no competing interests.

Author details

[1]School of Medicine, Nankai University, Tianjin 300110, China
[2]Department of Intensive Care, Tianjin Third Central Hospital, Tianjin 300170, China
[3]College of Environmental Sciences and Engineering, Nankai University, Tianjin 300350, China
[4]School of the Environment, Nanjing University, Nanjing 210046, China

Received: 19 September 2024 / Accepted: 26 March 2025
Published online: 09 May 2025

References

1. Charles MP, Kali A, Easow JM, Joseph NM, Ravishankar M, Srinivasan S, et al. Ventilator-associated pneumonia. Australasian Med J. 2014;7(8):334–44.
2. Papazian L, Klompas M, Luyt CE. Ventilator-associated pneumonia in adults: a narrative review. Intensive Care Med. 2020;46(5):888–906.
3. Kohbodi GA, Rajasurya V, Noor A, Ventilator-Associated, Pneumonia. StatPearls. Treasure Island (FL) ineligible companies. Disclosure: Venkat Rajasurya declares no relevant financial relationships with ineligible companies. Disclosure: Asif Noor declares no relevant financial relationships with ineligible companies.: StatPearls publishing copyright © 2024. StatPearls Publishing LLC.; 2024.
4. Bassetti M, Taramasso L, Giacobbe DR, Pelosi P. Management of ventilator-associated pneumonia: epidemiology, diagnosis and antimicrobial therapy. Expert Rev Anti-infective Therapy. 2012;10(5):585–96.
5. Keyt H, Faverio P, Restrepo MI. Prevention of ventilator-associated pneumonia in the intensive care unit: a review of the clinically relevant recent advancements. Indian J Med Res. 2014;139(6):814–21.
6. Estes RJ, Meduri GU. The pathogenesis of ventilator-associated pneumonia: I. Mechanisms of bacterial transcolonization and airway inoculation. Intensive Care Med. 1995;21(4):365–83.
7. Aragon D, Sole ML. Implementing best practice strategies to prevent infection in the ICU. Crit Care Nurs Clin N Am. 2006;18(4):441–52.
8. Chakradhar S. A curious connection: teasing apart the link between gut microbes and lung disease. Nat Med. 2017;23(4):402–4.
9. Dickson RP, Singer BH, Newstead MW, Falkowski NR, Erb-Downward JR, Standiford TJ, et al. Enrichment of the lung Microbiome with gut bacteria in sepsis and the acute respiratory distress syndrome. Nat Microbiol. 2016;1(10):16113.
10. Stanley D, Mason LJ, Mackin KE, Srikhanta YN, Lyras D, Prakash MD, et al. Translocation and dissemination of commensal bacteria in post-stroke infection. Nat Med. 2016;22(11):1277–84.
11. Wheatley RM, Caballero JD, van der Schalk TE, De Winter FHR, Shaw LP, Kapel N, et al. Gut to lung translocation and antibiotic mediated selection shape the dynamics of Pseudomonas aeruginosa in an ICU patient. Nat Commun. 2022;13(1):6523.
12. Messika J, Magdoud F, Clermont O, Margetis D, Gaudry S, Roux D, et al. Pathophysiology of Escherichia coli ventilator-associated pneumonia: implication of highly virulent extraintestinal pathogenic strains. Intensive Care Med. 2012;38(12):2007–16.
13. Fihman V, Messika J, Hajage D, Tournier V, Gaudry S, Magdoud F, et al. Five-year trends for ventilator-associated pneumonia: correlation between Microbiological findings and antimicrobial drug consumption. Int J Antimicrob Agents. 2015;46(5):518–25.

14. Drevinek P, Mahenthiralingam E. Burkholderia cenocepacia in cystic fibrosis: epidemiology and molecular mechanisms of virulence. Clin Microbiol Infect. 2010;16(7):821–30.
15. Mahenthiralingam E, Baldwin A, Dowson CG. Burkholderia Cepacia complex bacteria: opportunistic pathogens with important natural biology. J Appl Microbiol. 2008;104(6):1539–51.
16. Rea-Neto A, Youssef NCM, Tuche F, Brunkhorst F, Ranieri VM, Reinhart K, et al. Diagnosis of ventilator-associated pneumonia: a systematic review of the literature. Crit Care. 2008;12:1–14.
17. Qin N, Yang F, Li A, Prifti E, Chen Y, Shao L, et al. Alterations of the human gut Microbiome in liver cirrhosis. Nature. 2014;513(7516):59–64.
18. Reddy S, Hung L-H, Sala-Torra O, Radich JP, Yeung CC, Yeung KY. A graphical, interactive and GPU-enabled workflow to process long-read sequencing data. BMC Genomics. 2021;22:1–8.
19. Koren S, Walenz BP, Berlin K, Miller JR, Bergman NH, Phillippy AM. Canu: scalable and accurate long-read assembly via adaptive k-mer weighting and repeat separation. Genome Res. 2017;27(5):722–36.
20. Chen Z, Erickson DL, Meng J. Benchmarking long-read assemblers for genomic analyses of bacterial pathogens using Oxford nanopore sequencing. Int J Mol Sci. 2020;21(23):9161.
21. Hunt M, Silva ND, Otto TD, Parkhill J, Keane JA, Harris SR. Circlator: automated circularization of genome assemblies using long sequencing reads. Genome Biol. 2015;16:1–10.
22. Chen Z, Erickson DL, Meng J. Polishing the Oxford nanopore long-read assemblies of bacterial pathogens with illumina short reads to improve genomic analyses. Genomics. 2021;113(3):1366–77.
23. Li D, Liu CM, Luo R, Sadakane K, Lam TW. MEGAHIT: an ultra-fast single-node solution for large and complex metagenomics assembly via succinct de Bruijn graph. Bioinformatics. 2015;31(10):1674–6.
24. Segata N, Waldron L, Ballarini A, Narasimhan V, Jousson O, Huttenhower C. Metagenomic microbial community profiling using unique clade-specific marker genes. Nat Methods. 2012;9(8):811–4.
25. Jia B, Raphenya AR, Alcock B, Waglechner N, Guo P, Tsang KK, et al. CARD 2017: expansion and model-centric curation of the comprehensive antibiotic resistance database. Nucleic Acids Res. 2017;45(D1):D566–D573.
26. Yin X, Jiang XT, Chai B, Li L, Yang Y, Cole JR, et al. ARGs-OAP v2.0 with an expanded SARG database and hidden Markov models for enhancement characterization and quantification of antibiotic resistance genes in environmental metagenomes. Bioinformatics. 2018;34(13):2263–70.
27. Li B, Yang Y, Ma L, Ju F, Guo F, Tiedje JM, et al. Metagenomic and network analysis reveal wide distribution and co-occurrence of environmental antibiotic resistance genes. ISME J. 2015;9(11):2490–502.
28. Li H, Handsaker B, Wysoker A, Fennell T, Ruan J, Homer N, et al. The sequence alignment/map format and samtools. Bioinformatics. 2009;25(16):2078–9.
29. Kang DD, Li F, Kirton E, Thomas A, Egan R, An H, et al. MetaBAT 2: an adaptive Binning algorithm for robust and efficient genome reconstruction from metagenome assemblies. PeerJ. 2019;7:e7359.
30. Parks DH, Imelfort M, Skennerton CT, Hugenholtz P, Tyson GW. CheckM: assessing the quality of microbial genomes recovered from isolates, single cells, and metagenomes. Genome Res. 2015;25(7):1043–55.
31. Chen Y, Ye W, Zhang Y, Xu Y. High speed BLASTN: an accelerated megablast search tool. Nucleic Acids Res. 2015;43(16):7762–8.
32. Bottery MJ, Wood AJ, Brockhurst MA. Adaptive modulation of antibiotic resistance through intragenomic Coevolution. Nat Ecol Evol. 2017;1(9):1364–9.
33. Zhang P, Mao D, Gao H, Zheng L, Chen Z, Gao Y, et al. Colonization of gut microbiota by plasmid-carrying bacteria is facilitated by evolutionary adaptation to antibiotic treatment. ISME J. 2022;16(5):1284–93.
34. Sprouffske K, Wagner AJBB. Growthcurver: an R package for obtaining interpretable metrics from microbial growth curves. 2016;17(1).
35. Cooper HS, Murthy SN, Shah RS, Sedergran DJ. Clinicopathologic study of dextran sulfate sodium experimental murine colitis. Lab Invest. 1993;69(2):238–49.
36. Portal C, Gouyer V, Leonard R, Husson MO, Gottrand F, Desseyn JL. Long-term dietary (n-3) polyunsaturated fatty acids show benefits to the lungs of Cftr F508del mice. PLoS ONE. 2018;13(6):e0197808.
37. Oksanen J, Blanchet FG, Kindt R, Legendre P, O'Hara R. Package 'vegan'. 2010.
38. Dray S, Dufour A-B. The ade4 package: implementing the duality diagram for ecologists. J Stat Softw. 2007;22:1–20.
39. Wickham H. ggplot2. Wiley interdisciplinary reviews: computational statistics. 2011;3(2):180-5.
40. Jain C, Rodriguez-R LM, Phillippy AM, Konstantinidis KT, Aluru S. High throughput ANI analysis of 90K prokaryotic genomes reveals clear species boundaries. Nat Commun. 2018;9(1):5114.
41. Das S, Batra S, Rachagani S. Mouse model of dextran sodium sulfate (DSS)-induced colitis. Bio-Protocol. 2017;7(16).
42. Poovelikunnel TT, Barakat A, O'Hara A, Humphreys HJ, Newmann V, Talento AF. Are positive-pressure ventilation lobby rooms effective for protective and source isolation? J Hosp Infect. 2020;106(1):53–6.
43. Crnich CJ, Safdar N, Maki DG. The role of the intensive care unit environment in the pathogenesis and prevention of ventilator-associated pneumonia. Respir Care. 2005;50(6):813–36. discussion 36– 8.
44. Zhao T, Wu X, Zhang Q, Li C, Worthington HV, Hua F. Oral hygiene care for critically ill patients to prevent ventilator-associated pneumonia. Cochrane Database Syst Rev. 2020;12(12):Cd008367.
45. Nseir S, Di Pompeo C, Jozefowicz E, Cavestri B, Brisson H, Nyunga M et al. Relationship between tracheotomy and ventilator-associated pneumonia: a case–control study. Eur Respir J.30(2):314–20.
46. Güner CK, Kutlutürkan S. Role of head-of-bed elevation in preventing ventilator-associated pneumonia bed elevation and pneumonia. Nurs Crit Care. 2022;27(5):635–45.
47. Hamilton VA, Grap MJ. The role of the endotracheal tube cuff in microaspiration. Heart Lung. 2012;41(2):167–72.
48. Chen L-X, Anantharaman K, Shaiber A, Eren AM, Banfield JF. Accurate and complete genomes from metagenomes. Genome Res. 2020;30(3):315–33.
49. Lucero CA, Cohen AL, Trevino I, Rupp AH, Harris M, Forkan-Kelly S, et al. Outbreak of burkholderia Cepacia complex among ventilated pediatric patients linked to hospital sinks. Am J Infect Control. 2011;39(9):775–8.
50. Okimoto N, Hayashi T, Ishiga M, Nanba F, Kishimoto M, Yagi S, et al. Clinical features of Escherichia coli pneumonia. J Infect Chemotherapy: Official J Japan Soc Chemother. 2010;16(3):216–8.
51. Lagamayo ENJAjoic. Antimicrobial resistance in major pathogens of hospital-acquired pneumonia in Asian countries. 2008;36(4):S101–8.
52. La Combe B, Clermont O, Messika J, Eveillard M, Kouatchet A, Lasocki S, et al. Pneumonia-Specific Escherichia coli with distinct phylogenetic and virulence profiles, France, 2012–2014. Emerg Infect Dis. 2019;25(4):710–8.
53. El-Mokhtar MA, Daef E, Mohamed Hussein AAR, Hashem MK, Hassan HM. Emergence of nosocomial pneumonia caused by Colistin-Resistant Escherichia coli in patients admitted to chest. Intensive Care Unit. 2021;10(3):226.
54. Loutet SA, Valvano MA. Extreme antimicrobial peptide and polymyxin B resistance in the genus burkholderia. Front Cell Infect Microbiol. 2011;1:6.
55. Rhodes KA, Schweizer HP. Antibiotic resistance in burkholderia species. Drug resistance updates: reviews and commentaries in antimicrobial and anticancer chemotherapy. 2016;28:82–90.
56. Somprasong N, Hall CM, Webb JR, Sahl JW, Wagner DM, Keim P et al. Burkholderia ubonensis meropenem resistance: insights into distinct properties of class A β-Lactamases in burkholderia Cepacia complex and burkholderia Pseudomallei complex bacteria. mBio. 2020;11(2).
57. Lankelma JM, van Vught LA, Belzer C, Schultz MJ, van der Poll T, de Vos WM, et al. Critically ill patients demonstrate large interpersonal variation in intestinal microbiota dysregulation: a pilot study. Intensive Care Med. 2016;43(1):59–68.
58. Haghi F, Lohrasbi V, Zeighami H. High incidence of virulence determinants, aminoglycoside and Vancomycin resistance in enterococci isolated from hospitalized patients in Northwest Iran. BMC Infect Dis. 2019;19:1–10.
59. Mu S, Xiang H, Wang Y, Wei W, Long X, Han Y, et al. The pathogens of secondary infection in septic patients share a similar genotype to those that predominate in the gut. Crit Care. 2022;26(1):68.

Publisher's note